Journal of Sound and Vibration 329 (2010) 2083–2098

Contents lists available at ScienceDirect

Journal of Sound and Vibration

journal homepage: www.elsevier.com/locate/jsvi

Effect of sensor proximity over the non-conformal hologram plane in the near-field acoustical holography based on the inverse boundary element method

Agustinus Oey, Hae-Won Jang, Jeong-Guon Ih *

Center for Noise and Vibration Control (NoViC), Department of Mechanical Engineering, KAIST, Daejeon 305-701, Republic of Korea

ARTICLE INFO

Article history:
Received 7 April 2009
Received in revised form
18 November 2009
Accepted 8 December 2009
Handling Editor: Y. Auregan
Available online 31 December 2009

ABSTRACT

Near-field acoustical holography (NAH) is a useful tool for the identification and visualization of vibro-acoustic sources. In particular, NAH can be applied to many practical sources having irregular shape if the inverse boundary element method (BEM) is employed. Once the relation between the source and the radiated field is defined in the transfer matrix modeled by the BEM, the reconstruction of acoustic parameters on the source surface can be conducted by the multiplication of the inverse transfer matrix and the field data measured over the hologram surface. The usual practical way to measure the field data radiated from an irregular shaped source is to adopt a regular hologram surface, which can be a flat, cylindrical, or spherical shape, for the measurement ease. Then, the hologram surface is not conformal to the source surface and the resulting transfer matrix becomes further ill-posed than the conformal case. To investigate the effect of sensor proximity and distance variability on the reconstruction error, simulation and measurement were conducted for an interior problem comprised of a parallelepiped rigid box with a vibrating end plate. Flat, tilted, and randomized hologram surfaces were adopted in the test. It was shown that the reconstruction error is greatly affected by the conditioning of transfer matrix which is related to the positioning of sensor. To improve the reconstruction accuracy, an investigation was conducted to find proper field points among a large number of overdetermined field points. The number of field data was reduced gradually under various reduction schemes using condition number, effective independence value, and sensor distance. It was demonstrated that the quality of reconstruction result given by the non-conformal measurement can be improved by removing some field points that contribute to the ill-conditioning of the inverse problem. A small improvement of the reconstruction accuracy was observed by reducing the field points in the overdetermined situation. However, further reduction of the field points, becoming an underdetermined situation, yielded a drastic improvement of the reconstruction accuracy.

1. Introduction

Near-field acoustical holography (NAH) is one of the inverse problems, of which the purpose is to recover the acoustical source parameters from the measured field data. Although the source surface and sound field are continuous, the

* Corresponding author. Tel.: +82 42 350 3035; fax: +82 42 350 8220.
E-mail address: J.G.Ih@kaist.ac.kr (J.-G. Ih).

0022-460X/$ - see front matter © 2009 Elsevier Ltd. All rights reserved.
doi:10.1016/j.jsv.2009.12.013

discretized source surface and the sound field should be considered for the practical computation and measurement. During the inverse calculation process, a small portion of noise contained in the field data measured at the hologram surface will be amplified and interfere with the true signals. These amplified spurious signals from noises spoil the accuracy of the reconstruction. A high sensitivity to the small change in the field data together with the limited resolution of the field data would yield the indefinite solution for the source parameters. In such numerically unstable circumstances, the transfer matrix is often ill-conditioned.

An ill-conditioned transfer matrix is characterized by a large condition number that numerically indicates the existence of linearly dependent vectors. The physical meaning in relation to the NAH is that the information measured by the sensors, which experimentally defined on the hologram surface, is not complete and unique. However, when we tackle a practical problem, it is not *a priori* known whether the boundary element method (BEM) matrix will be a well-conditioned or an ill-conditioned one [1]. Main factors contributing to the ill-conditioning of the transfer matrix are geometrical setup of the system, signal-to-noise ratio (SNR) of the field data, spatial resolution of the source surface, number of field points, computational precision, etc. In this regard, the selection of the hologram surface shape, the location of measurement points on the hologram surface, and the spatial distribution of measurement points on the hologram surface are important in the implementation of NAH.

Near-field measurement is greatly helpful in enhancing the SNR of the field signals. Also, a close near-field measurement, far closer than the Rayleigh distance [2], is beneficial to the inverse source reconstruction in the viewpoint of collecting signals having evanescent waves in a rich content. Those evanescent waves contain the detailed information on the source activity although they are non-propagating to the far field. By including the evanescent waves, in other words high order wave vectors, as much as possible, one can reconstruct source parameters with a good precision, thus fulfilling the source identification of extended irregular source. The recovered source parameters over the source surface field can be used for an accurate prediction of the acoustic pressure and energy quantities everywhere from near field to far field as a post processing. To detect as many high order wave vectors as possible and to catch almost all the radiation energy, the hologram surface enclosing the source surface should be comprised of many measuring points. In the near-field, one can measure the field data over a much smaller hologram surface area than the far field, thus reducing the number of measurement points.

As stated earlier, the field data must be recorded at the hologram surface which is sufficiently close to the source surface, so that the signal strength of the evanescent wave falls within the dynamic range of the sensor [3]. However, in applying the BEM-based NAH to practical situations, the minimum distance between source point and sensor should be carefully selected. The reason is that the conventional BEM-based NAH without any numerical treatment suffers from a hyper-singularity in the close near-field of the source surface. Hyper-singularity limits the minimum measurement distance to one-fifth of the characteristic length of the boundary element model [4]. This problem can be alleviated by using the nonsingular or weakly singular boundary integral formulation [5]. It is also important to keep the measurement position exactly as given in the model. Position mismatch of the sensor will amplify the random error in the backward problem [6].

Even for a simple hologram surface, the distances between sensors and their nearest points of the source surface are not usually the same if a perfectly conformal hologram surface to the irregularly shaped source is not chosen. Due to the exponential decay of evanescent waves, the disparity in the information on the propagating and the non-propagating waves captured by sensors at different positions will affect the reconstruction error. Therefore, it is important to understand the effect of sensor proximity and distance variability on the reconstruction error because the arrangement of a perfectly conformal hologram surface is not practical for most practical irregular-shaped sources. In this study, a numerical check on the relation between the source-to-sensor distance and the reconstruction quality is followed by an investigation on the effect of non-conformal hologram surface to the ill-conditioning of the transfer matrix. It is also studied that the reconstruction error depends on the selection method for the field points on the non-conformal hologram surface. From the study result, the best scheme in selecting effective sensor positions is suggested to minimize the reconstruction error. Simulation and experiment of interior problem are compared for validation and demonstration.

2. Formulation of BEM-based NAH

Consider a three-dimensional interior or exterior domain V enclosed by the boundary surface S_o filled with the isothermal, homogeneous, inviscid, compressible, and stationary fluid medium. Acoustic field pressure satisfying Neumann, Dirichlet, or impedance boundary conditions can be obtained by Kirchhoff–Helmholtz integral equation as follows [7]:

$$c(\mathbf{r})p(\mathbf{r}) = \int_{S_o} \left[G(\mathbf{r},\mathbf{r}_0)\frac{\partial p(\mathbf{r}_0)}{\partial \mathbf{n}(\mathbf{r}_0)} - \frac{\partial G(\mathbf{r},\mathbf{r}_0)}{\partial \mathbf{n}(\mathbf{r}_0)} p(\mathbf{r}_0) \right] \mathrm{d}S(\mathbf{r}_0). \tag{1}$$

Here, $\mathbf{r}$, $\mathbf{r}_0$ denotes the position vector of the field point and surface point, respectively, $p(\mathbf{r}_0)$ denotes the pressure over the source surface, $G(\mathbf{r},\mathbf{r}_0) = \exp(-jkR)/R$ is the three-dimensional free-space Green function, $R = |\mathbf{r}-\mathbf{r}_0|$ is the distance between field point and surface point, $\partial/\partial\mathbf{n}$ means the outward normal derivative on the surface, and the leading coefficient $c(\mathbf{r}) = 4\pi + \int_{S_o} \frac{\partial}{\partial \mathbf{n}(\mathbf{r}_0)} \left(\frac{1}{R}\right) \mathrm{d}S(\mathbf{r}_0)$ represents the radiation or solid angle formed by the enclosing three-dimensional surfaces around the boundary point at $\mathbf{r}_0$ looking into an observation, or field, point $\mathbf{r}$. The discrete form of Eq. (1) is given

by

$$\mathbf{D}_S\mathbf{p}_S = \mathbf{M}_s\mathbf{v}_s, \quad \mathbf{p}_f = \mathbf{D}_f\mathbf{p}_S + \mathbf{M}_f\mathbf{v}_s, \tag{2,3}$$

where $\mathbf{p}_s$, $\mathbf{v}_s$ are the surface pressure and normal velocity, $\mathbf{D}_s$, $\mathbf{M}_s$ mean the dipole and monopole matrices on the source surface, and $\mathbf{p}_f$, $\mathbf{D}_f$, $\mathbf{M}_f$ are those corresponding to the field, respectively [8]. The matrix equation includes solid angle information in $\mathbf{D}_s$.

If it is assumed that the Neumann boundary conditions can be applied to the problem and the ${\mathbf{D}_s}^{-1}$ exists, the relation between field pressure and surface normal velocity can be expressed as

$$\mathbf{p}_f = (\mathbf{D}_f\mathbf{D}_s^{-1}\mathbf{M}_s + \mathbf{M}_f)\mathbf{v}_s \equiv \mathbf{G}_v\mathbf{v}_s. \tag{4}$$

Here, $\mathbf{G}_v$ is the vibro-acoustic transfer matrix or complex frequency response functions correlating the surface normal velocity and the field pressure that contains the geometric information of the system as well. Then, by means of singular value decomposition, the inverse problem can be formulated as

$$\mathbf{v}_s = (\mathbf{G}_v^H\mathbf{G}_v)^{-1}\mathbf{G}_v^H\mathbf{p}_f \equiv \mathbf{G}_v^+\mathbf{p}_f, \tag{5}$$

where $\mathbf{G}_v^+ \cong \mathbf{W}\mathbf{\Lambda}^{-1}\mathbf{U}^H$, is the pseudo-inverse of $\mathbf{G}_v$. The singular values represented by $\mathbf{\Lambda}$ can be considered as the singularity index of the transfer matrix, $\mathbf{W}$ and $\mathbf{U}$ represent the contribution of the corresponding vibration mode on the source surface to the propagation mode in the acoustic field. The acoustic modes with small singular values are related with the non-propagating wave vectors.

The solution in Eq. (5) inherits an ill-posed inverse problem due to a cluster of small singular values that its inverse includes strong amplification of a very small signal at high frequency components. Consequently, the solution becomes very sensitive to noise and measurement error resulting in large reconstruction error in the backward calculation. If the measurement noise, $\mathbf{n}$, coexists with the true signal and it is assumed as the uncorrelated Gaussian random type noise having zero mean and variance σ^2, the expected squared-value of reconstruction error is given by

$$E[(\mathbf{v}_S - \hat{\mathbf{v}}_S)^H(\mathbf{v}_S - \hat{\mathbf{v}}_S)] \equiv \sigma^2 S_F, \tag{6}$$

where $\hat{\mathbf{v}}_S = \mathbf{G}_v^+(\mathbf{p}_f + \mathbf{n})$ is the estimated source velocity and $S_F = tr\{\mathbf{G}_v^H\mathbf{G}_v\}^{-1}$ represents the singularity factor that indicates the degree of singularity of $\mathbf{G}_v$. As shown by the equation, the reconstruction error is in proportion to the measurement noise variance and singularity factor of transfer matrix. To solve the problem, regularization techniques have been developed to refine the reconstruction image to an acceptable level (for example [9–11]).

3. Evanescent waves in acoustical holography

In the acoustical holography, the amount of source information becomes small as the measurement plane becomes more distant from the source. Due to this reason, selection of the hologram surface in the near-field is preferred because the radiated field which is rich in information on the source activity can be measured including the evanescent waves. For having the same statistical condition of error, it is also preferred that the distance between a source point and a nearest measurement point is same for any source point, which eventually suggests a conformal hologram surface. Obviously, conformal measurement is able to provide a superior visualization of the noise source [12]. This is true in general, but, in many practical irregular sources, a conformal hologram surface cannot be realized because of the difficulty in sensor positioning.

3.1. Conformal hologram surface

A parallelepiped box having dimensions of 0.5 m (w) × 0.5 m (h) × 1.5 m (l) was selected to test an interior problem. All walls except the vibrating plate clamped at one end of the box were assumed rigid. The corresponding BEM model was composed of 1402 nodes and 2800 linear triangular elements, which has the largest characteristic length of 0.072 m. Based on the λ/6-criterion, the high frequency limit was 800 Hz and the expected maximum modeling error was less than 5% [13]. The hologram surface was arranged in parallel with the plate. There were 81 nodes on the plate and 81 field points on the hologram surface. The nodes and the field points were equally spaced.

The cutoff frequency of the plane wave propagating inside the cavity was about 340 Hz. Near to or lower than this cutoff frequency, three cavity resonance frequencies existed at 114, 229, and 343 Hz. The steel plate of 1 mm in thickness was a subject to the harmonic point excitation. For the data preparation, first, the velocity distribution on the vibrating plate was computed using a commercial FEM platform. The plate was uniformly discretized into a grid of 11 by 11 points and the fixed boundary condition was assumed. By neglecting the acousto-structural interaction, the interior sound field was computed by using the BEM. Fig. 1 displays the acoustic field on a planar section at z=0.25 m, corresponding to the (3,3) vibration mode at 213 Hz. One can see that the evanescent wave occupies in the vicinity of the vibrating plate and dies out shortly at some distance. The majority of the field is dominated by the plane wave.

Fig. 2 shows two examples of reconstruction result recovered from the hologram data at two different distances from the vibrating plate: 0.03λ and 0.25λ. In the reconstruction process, the Tikhonov regularization technique combined with

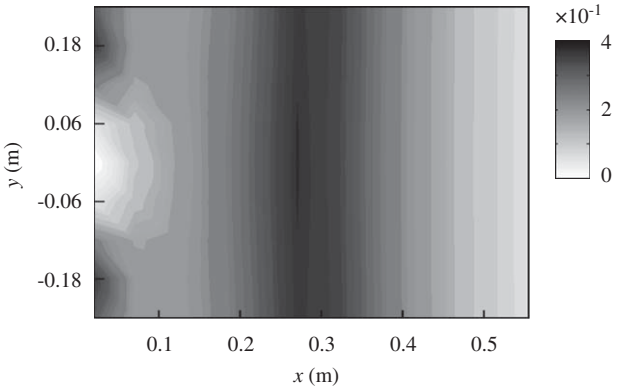

Fig. 1. Field pressure distribution at 213 Hz over a plane along the axial direction x at z=0.25 m. The plane wave starts to form when x is larger than about 0.15 m; whereas the evanescent wave dominates the region in the vicinity of the vibrating plate (x=0).

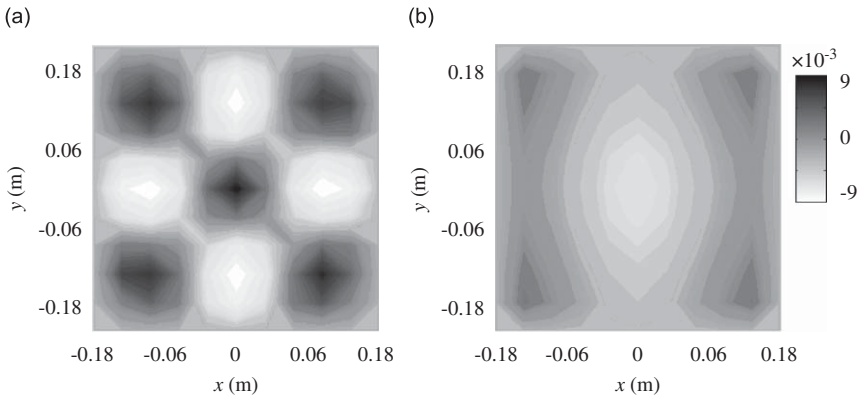

Fig. 2. Reconstructed surface velocities recovered from the field data apart from the source surface by: (a) 0.03λ (d=0.05 m, e=17.1%, MAC=0.97) and (b) 0.25λ (d=0.4 m, e=93.9%, MAC=0.12).

the generalized cross validation (GCV) method was employed [14–15]. The reconstruction error was quantified by two different measures: the L2-norm error, e (percent), and the modal assurance criterion, MAC. They are defined as

$$e = \frac{\|\mathbf{v}_S - \hat{\mathbf{v}}_S\|_2}{\|\mathbf{v}_S\|_2} \times 100, \quad \text{MAC} = \frac{|\mathbf{v}_S \hat{\mathbf{v}}_S|^2}{|\mathbf{v}_S|^2 |\hat{\mathbf{v}}_S|^2}. \tag{7,8}$$

One should note that e accounts for the overall error and MAC implies the shape correlation between the actual and the reconstructed surface normal velocity distribution [16]. Reconstruction errors were calculated in Monte-Carlo simulation scheme using 1000 samples of field data, synthesized by adding a small amount of Gaussian random noise to the calculated sound pressure. The signal-to-noise ratio (SNR) of all data sets was maintained to be 20 dB. An accurate reconstruction result can be observed in Fig. 2(a), which was recovered from a very close near-field data measured at a distance less than 0.1λ. As the hologram surface moves further apart from the source surface, the reconstruction error becomes large even in the range that can be considered as near-field. A typical reconstructed example is shown in Fig. 2(b), which was recovered from the field data located at 0.25λ. One can find that the restored source shape looks like a corner mode. Beyond about 0.25λ, the plane wave propagates dominantly and any useful detailed source information cannot be recovered. As depicted by simulation result, the amount of evanescent waves contained in the field pressure data is very crucial for the precise reconstruction of the source. Therefore, one should put the sensors as close to the source surface as possible, which is also beneficial in maintaining a high SNR. From the other view, when the hologram surface includes sensors at different source-to-sensor distances, each of the sensors contains a different degree of source information. This means that the reconstruction result will be affected with the variability of source-to-sensor distance.

3.2. Non-conformal hologram surface

In principle, because the surface of conformal hologram follows the shape of the source surface, the signal quality of the field data measured over the conformal hologram surface should be the same. This is true provided that the noise added to the signal is uniformly distributed over all measurement points and there is no other sound source. However, the usual

practical way to measure the field data radiated from an irregular shaped source is to adopt a simple hologram surface, such as flat, cylindrical, or spherical shapes, for the measurement ease. Then, the hologram surface is no longer conformal to the source surface and the resulting transfer matrix becomes further ill-posed than the conformal hologram surface case. Because the distances between the source surface and the nearest measuring point are various in the measurement of an irregular shaped source, the reconstruction error associated with such spatial variation of measuring distances should be investigated for the actual applications.

To investigate the effect of non-conformal hologram data, the same parallelepiped box used in Section 3.1 was employed as a test example. Instead of using a pair of irregularly shaped source and flat hologram surface as a test example, a pair of flat source surface and irregularly shaped hologram surface can be adopted in the investigation without loss of the nature of the problem. Limiting the frequency range below 400 Hz, a simple BEM model comprised of 365 nodes and 726 linear triangular elements could be built, of which 49 nodes were defined on the vibrating plate located at one of the box ends. The other parts were assumed as rigid. Fig. 3(a) shows the BEM model and dimension of the parallelepiped box.

Randomized hologram surface was chosen to represent the irregularly shaped hologram surface. It was positioned inside the box, very near to the plate but no closer than 0.03 m. The reason behind the use of randomized field points was to investigate the relation between the variation of source-to-sensor distances and the conditioning of transfer matrix in a statistical manner. A large number of random hologram planes can be generated easily, in which the control variable is the distance between the source surface and the mean sensor position in the normal direction to the nearest source surface, viz., along the x-direction in Fig. 3. One should also note that, in many practical situations in dealing with irregular shaped sources, shoebox or cylindrically shaped hologram surface is usually selected as the hologram surface. In such conditions, separation distances between source points and nearest sensors tend to be distributed in a random manner approximately. By changing the source-to-sensor distance in the normal direction to the nearest plate surface, 30 different sets of randomized hologram surfaces were generated in accordance with the Gaussian random distribution specified with statistical parameters of mean value, μ, and variance, σ_d^2. Each set contained 49 field points or sensors, in which the source-to-sensor distances are arranged to be in a normal distribution. First, each measuring distance of 49 field points was selected within the distance range, d, by the Gaussian random distribution. This distance range is actually related to the minimum and maximum distances of tilted hologram plane, which is discussed later in Section 4.2. Then, each calculated distance was assigned to a grid position which was also randomly selected without any overlap. The final data set contained 180 randomized hologram surfaces for 6 combinations of mean value and variance. In addition, flat hologram surfaces corresponding to the mean values of the random data sets were prepared for comparison purpose. Fig. 3(b)–(d) illustrate three typical arrangements of the flat, tilted, and randomized hologram surfaces, respectively.

The singularity factors and the condition numbers of the transfer matrices in Eq. (4) are plotted in Fig. 4(a) and (b), respectively. It should be recalled that the transfer matrix defines the relationship between the surface normal velocity on the source surface and the acoustic field pressure on the hologram surfaces. There are three curve groups which are

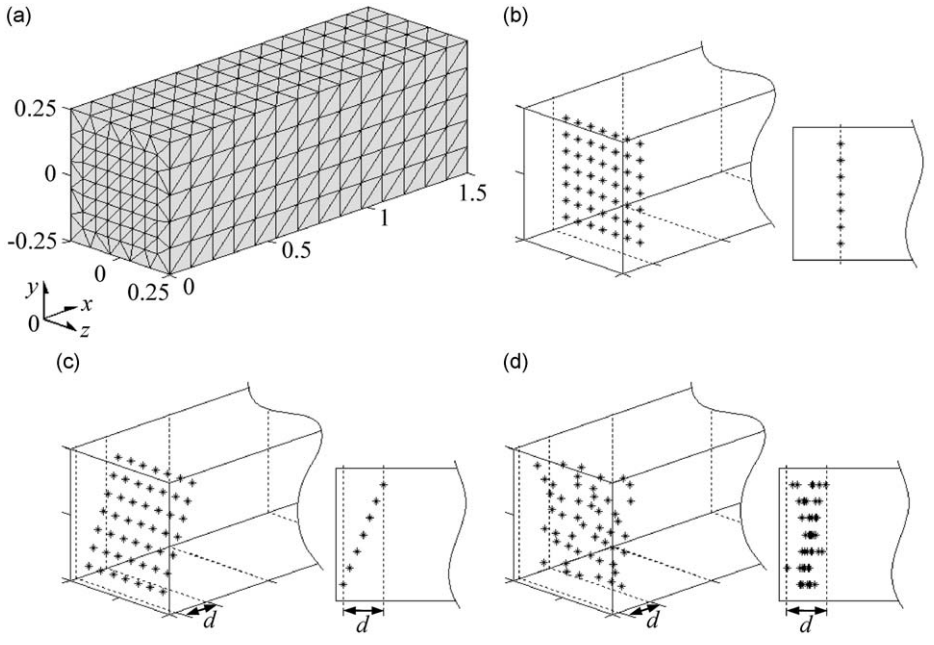

Fig. 3. (a) Boundary element model of a parallelepiped box adopted as the test example. Arrangements of field points on typical three hologram surfaces: (b) flat, (c) tilted, and (d) randomized.

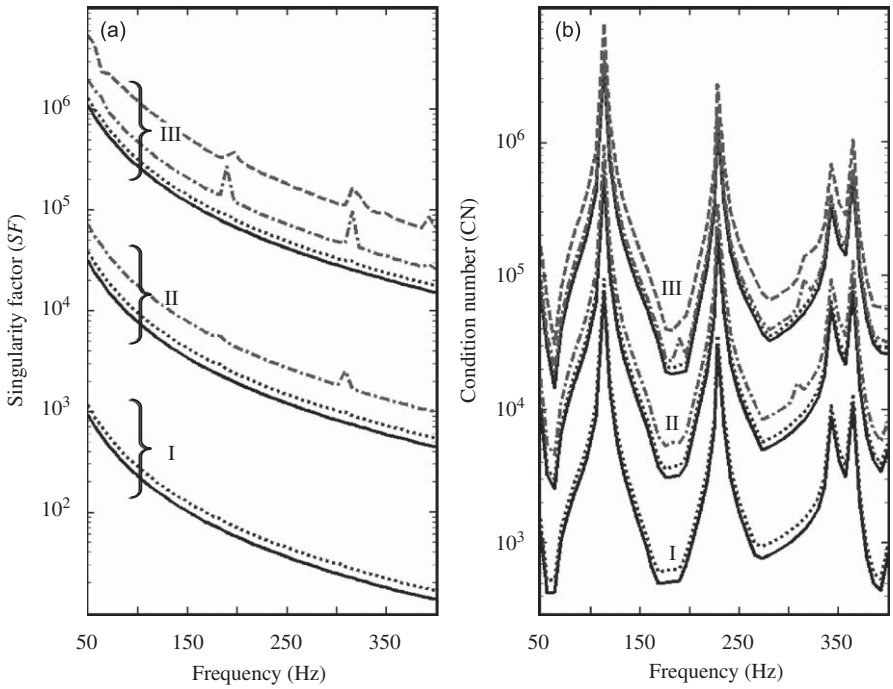

Fig. 4. Ill-posedness of the transfer matrix for flat and randomly shaped hologram surfaces: (a) singularity factor and (b) condition number. A curve group was calculated for the same mean distance (for group I, μ=0.06 m; for group II, μ=0.09 m; for group III, μ=0.12 m), while various line styles denote the difference in distance variance (——, $\sigma_d^2=0$; ·····, $\sigma_d^2=0.01$; -·-·-·, $\sigma_d^2=0.03$; – – –, $\sigma_d^2=0.07$).

different in the mean distance: 0.06, 0.09, and 0.12 m. For each group, the calculated singularity factors and condition numbers of the transfer matrix of hologram surfaces having randomly distributed points are compared with those of the flat hologram surfaces at mean distances. Black solid lines belong to the flat hologram surfaces. The other lines, i.e., dotted, lined and dotted, and dashed lines, were calculated for the hologram surfaces having randomly distributed points, at which the same mean value with the flat hologram surface were maintained. The difference between these lines is the distance variance. The singularity factor increases exponentially when the variance of sensor-to-source distance becomes larger. Naturally, as the variance becomes small, the singularity factor converges to that of the flat hologram surface. A similar trend can be seen in the condition number plot in Fig. 4(b). In addition, condition numbers grow rapidly to a large value at cavity resonance frequencies, 114, 228, and 343 Hz, at which the standing waves dominate the field, masking the directly radiated waves from the vibrating plate.

Because the distance variance, viz., the distance variability, can be thought of as a statistical measure of non-conformality, an error amplification factor can be defined as a ratio of the singularity factor of non-conformal hologram and conformal (or flat) hologram surfaces as

$$A_{\mathrm{SF}}=\frac{S_F}{S_{\mathrm{Fc}}}. \tag{9}$$

Here, S_{Fc} and S_F denote the singularity factors of the transfer matrices associated with the conformal and non-conformal hologram surfaces, respectively. The non-conformal hologram surface is statistically characterized with the mean distance, μ, and the variance, $\sigma_d^2>0$. The conformal hologram surface has zero variance but shares the same mean distance. Eq. (6) can be rewritten for taking account of the contribution from non-conformal hologram surfaces as

$$E[(\mathbf{v}_S-\hat{\mathbf{v}}_S)^H(\mathbf{v}_S-\hat{\mathbf{v}}_S)]\equiv\sigma^2 A_{\mathrm{SF}}S_{\mathrm{Fc}}. \tag{10}$$

It can be inferred here that the distance variability amplifies reconstruction error.

The trend of the error amplification is depicted in Fig. 5. Using a reference S_{Fc} value obtained from a flat hologram plane at 0.03 m, the error amplification factor, A_{SF}, was computed for 15 sets of 50 randomized hologram surfaces having different mean distances. The minimum distance from the source surface was fixed as 0.03 m for all 15 sets. This near-field distance is slightly larger than $\frac{1}{5}$ of the characteristic length of boundary elements, 0.143 m, that would not be influenced from the hyper singularity of the conventional direct BEM [5]. In selecting a set of hologram surface, 15 different maximum distances were initially given in the range 0.04–0.18 m with a step of 0.01 m, so the mean distances of 15 sets are different from each other. Then, a random number generation in between -1 and 1 for 49 points was conducted with the variance of 1. The source-to-hologram surface distance of each field point on the hologram surface can be obtained by mapping these random numbers onto the actual distance range given by minimum and maximum distances. One can calculate the

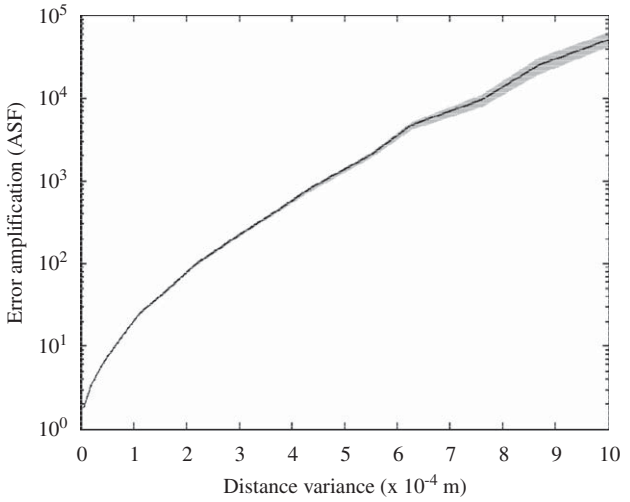

Fig. 5. Error amplification factor (A_{SF}) contributed from the variation of source-to-sensor distances. The grey area represents the scatter range of A_{SF} for 50–400 Hz, while the solid black line denotes the spectral average of A_{SF}.

actual variance for this set. The same procedure was repeated for the other sets of the hologram surfaces having different maximum distances to obtain the variance. As a result, the variances were ranged in between 10^{-4} and 10^{-3} in the choice of measurement set. Under a fixed value of variance for each set, the measuring distances at evenly distributed sensor positions were assigned differently, again, by a random fashion resulting 50 different hologram surfaces for each set. In Fig. 5, one can find that the overall trend or mean value of A_{SF} increases with σ_d^2 value. This means the singularity of the system, or in other word, the reconstruction error, will increase almost linearly with the increase of variance as the source-to-sensor distance varies from a uniform values, viz. conformal hologram shape.

4. Proper selection of field points

As discussed above, the reconstruction by using a non-conformal hologram surface suffers from the inaccuracy caused by the amplification of singularity of the transfer matrix compared to the conformal holography. Geometrical setup of the field points is definitely one of the important factors in the calculation of transfer matrix. Therefore, in the situation where the conformal hologram surface is not feasible to be adopted in the NAH, field points should be arranged in a way that provides the lowest singularity factor for a given condition of numbers of source points and field points. An excess number of field points are not always favorable because of the increasing measurement effort and the fact that most of measurement information will be discarded by the regularization process. One can recall that, at low frequency or for low order modes, the required number of field points to figure out the complete source information is small [17].

There are several techniques to select the field points properly [17–20]. The simplest way is to combine a number of field points to result a small condition number. In this method, first, one should generate a mother population of m candidate field points and calculate all possible transfer matrices relating n source points to $(m-1)$ field points. This can be done efficiently by manipulating $\mathbf{D}_f$ and $\mathbf{M}_f$ in Eq. (4). Then, take the average of condition numbers over the frequency range of interest and select any combination that has the smallest average. Repeat the procedure M times to select $(m-M)$ field points until the number meets the predetermined number of field points. In a similar way, the composite condition number technique [19] can be used to reduce the computation time.

Alternatively, the effective independence (EfI) method can be employed to select the field points that make the wave vectors to be as linearly independent as possible for a given number of points. The contribution of a single field point or a group of field points can be determined by the following EfI value [20]:

$$E_f = \mathrm{diag}\{\mathbf{U}\mathbf{U}^H\}. \tag{11}$$

Here, $\mathbf{U}$ is a unitary matrix having a propagation wave vector in each row as described in Eq. (5). At each calculation step, one can discard a single field point or a group of field points that exhibit the smallest EfI value. Then, EfI value of the remainder field points can be recalculated again with Eq. (11) and additional linearly dependent field point(s) can be further removed. The process is repeated until the number of remaining field points reaches the predetermined number.

4.1. Numerical simulation

To reconstruct the source field at 49 boundary nodes, 4 data sets having 98 field points for each set were considered as the mother populations or the initial candidate points. Each candidate data set was randomly prepared to possess the same

mean value and variances of the sensor-to-source distance along the x-direction. From these populations, field points were removed one by one, or group by group, until it reach the predetermined number of field points by considering the changes in condition number or EfI value. In this test example, 35 field points were used as the target number of points, which are smaller than the number of source nodes of the BEM model. Therefore, during the reduction process, the number of effective field points was progressively changed from 98 to 35 passing through 49, leading the input–output condition to migrate from overdetermined to underdetermined situation. However, in terms of field point density criterion, 35 field points still satisfy the Nyquist criterion as the ratio is larger than 3 sensors per wavelength. Reconstruction error for the reduced field data set at each stage was calculated without regularization using 50 samples of field pressure data with the SNR of 20 dB. It should be mentioned that, although this amount of noise contamination is seemingly not too much severe, it is a satisfactory amount to see the effect of noise clearly. One can recall the fact that, even for the SNR of 30 dB, the inverse process was certainly affected from the presence of environmental or measurement noise [21].

Evolution of reconstruction condition in terms of the average condition number of the transfer matrices, average error norms, and average MAC value is shown in Fig. 6 with the reduction of the number of field points. Reduced field points were selected by successively discarding the point with large condition number or with small EfI value. Two different spectral conditions of the vibrating plate were considered in the test: 86 and 128 Hz corresponding to (2,2) and (2,3) modes, respectively. One can find that the condition number of the system matrix decreases in general as the number of field points decreases by the repeated application of the reduction method using CN or EfI values. One can observe that CN increases a bit at some reduction stages when the EfI technique is employed. However, until reaching the same number of field points with the source nodes, the improvement of system condition number or reconstruction errors using either of these data reduction techniques does not seem to be prominent. This might be due to the fact that the benefit of using large redundant field points is not great in recovering the low order vibration modes due to the simplicity of mode shapes. One can observe a sudden increase of CN and error when the number of field points coincides with the number of source points. This also causes a degradation of MAC value at such a condition. An explanation on this phenomenon is given in Appendix A. The change in error norm with the reduction of field data exhibits a slightly increasing trend, but the rate is very small regardless of the frequency. Conversely, the change in MAC value with the reduction of field data shows a slightly decreasing trend, but, again, the rate is also very small regardless of the frequency. During the data reduction procedure, it is found that the removed field points were not always selected from the points located far apart from the source surface and they were varied with frequency. This may be explained by the fact that the redundant nature of a point in a set of

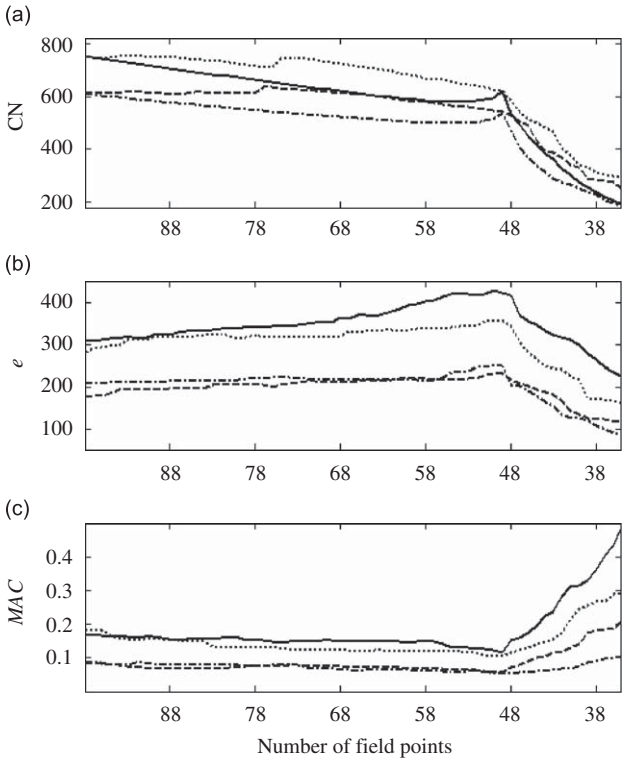

Fig. 6. Evolution of reconstruction condition using the ensemble average of three indicators: (a) condition number (CN) of the system matrix, (b) error norm (e) in %, and (c) MAC score. Field points were selected by successively discarding the point with large condition number or with small EfI value. Selected by using condition number: ———, 86 Hz, (2,2); - - - -, 128 Hz, (2,3). Selected by using EfI value: ·····, 86 Hz, (2,2); — — —, 128 Hz, (2,3). Error norm and MAC score were calculated without regularization.

measurement points is not only determined by the distance from the source surface, but it is also influenced from the degree of dependency of a point to the other points and the field condition including the reactivity.

4.2. Experiments

An experiment was conducted using a parallelepiped box with a vibrating endplate, which was similar to the box described in the numerical investigations. Except for the endplate, all the box walls were made of 1 in thick MDF panel, which was reinforced by a steel frame. The vibrating endplate was a 1 mm thick steel plate clamped around all edges and it was excited by an electro-dynamic shaker (B&K4809) at a point near a corner to avoid the nodal excitation or to invoke the multimodal excitation. Force transducer (Endevco 2312) was used to measure the excitation force and accelerometers (PCB 353B16) were employed to measure the surface normal velocities at 49 evenly spaced points on the vibrating surface.

Because the selection of sensor positions in a truly random way, as used for the simulation in Section 3.2, was difficult to do in practice, the experiment was conducted using the flat hologram plane varying the tilting angle as shown in Fig. 3(c), which was designed to have a close statistical meaning with the randomized field point arrangement as far as possible. In fact, the singular value and the condition number distributions calculated from random and titled hologram surfaces were found to behave in a similar trend. Two cases representing different degree of distance variability were prepared. In the first case, a tilted hologram plane with a 9° slope was positioned between 0.03 m (nearest distance in the lower side of the tilted plane) and 0.09 m (farthest distance in the upper side of the tilted plane) in the axial direction, while the tilted angle of the second case was 18°, located between 0.03 and 0.18 m. Sound pressures at 49 evenly spaced field points on these hologram surfaces were scanned by using an array comprised of 7 microphones (B&K 4935). An extra microphone was fixed at a field position, being used as the reference microphone for phase. In addition, the field pressures on a flat hologram surface located at 0.03 m was also measured for comparison purpose. Fig. 7 shows the measurement result at 86 Hz. In comparison with the flat hologram surface, the field pressure image over the tilted hologram planes shows relatively smeared phase information, in particular at the position far from the source surface. As one can expect, the tilted hologram data resulted in a degraded mode shape of the source vibrations as can be seen in Fig. 8. Tikhonov and GCV regularization scheme was employed, but it did not greatly improve Fig. 8(c) and (d).

It was thought that the quality of the reconstructed surface velocities in Fig. 8 can be improved by removing some field points that contribute more to the ill-conditioning of the transfer matrix. In this regard, three strategies for selecting field points were compared. The three strategies were based on the source-to-sensor distance, condition number, and Efl value. In the selection procedure, it was tried to maintain 35 field points from the tilted hologram planes. Fig. 9 shows the result

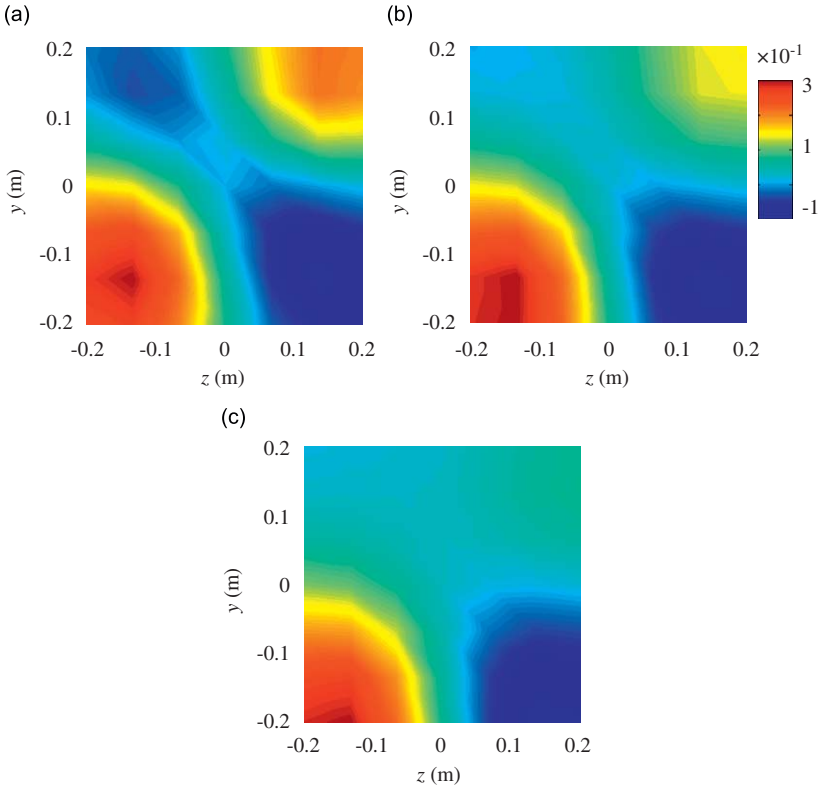

Fig. 7. Normalized field pressure at 86 Hz measured on three different hologram surfaces: (a) flat, (b) tilted (9°), and (c) tilted (18°).

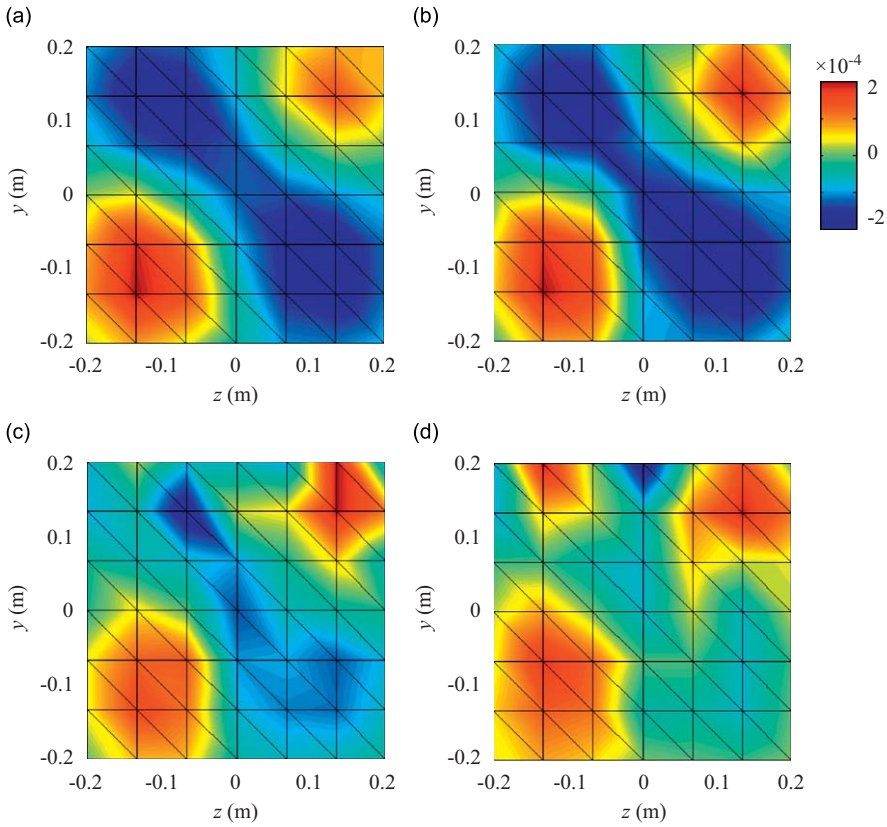

Fig. 8. (a) Measured source velocity showing the (2,2) mode at 86 Hz. Reconstructed source velocity calculated with regularization scheme given from: (b) flat hologram surface at 0.03 m (e=26%, MAC=0.97); (c) 9°-tilted hologram surface (e=32%, MAC=0.63); (d) 18°-tilted hologram surface (e=2200%, MAC=0.00).

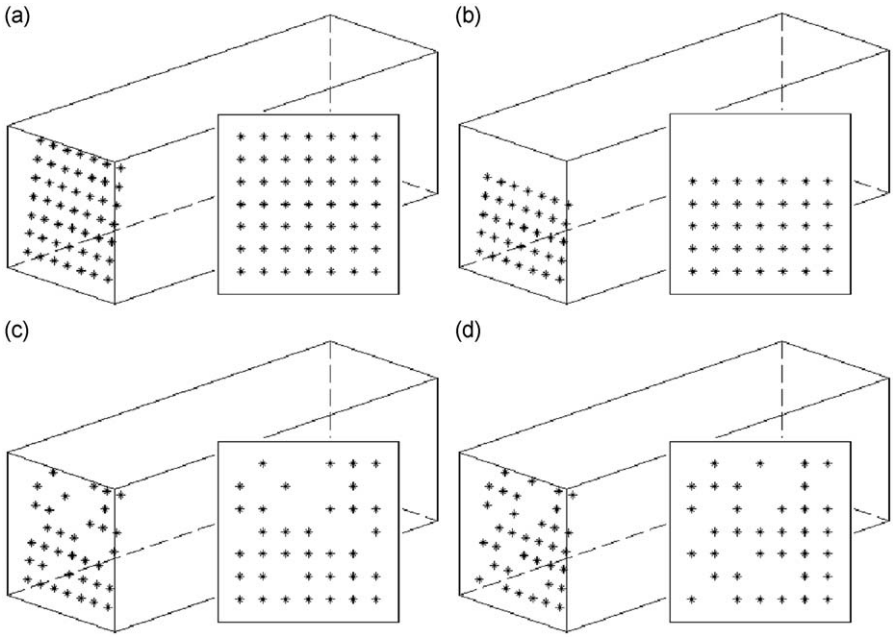

Fig. 9. (a) Initial setup of 49 field points on the 9°-tilted hologram plane. Final arrangements of 35 field points given by the selection process based on: (b) farthest distance, (c) largest condition number, (d) smallest EfI value.

for the 9°-tilted hologram plane. One can observed that the process based on the condition number removed most of the field points located at the farthest distance, while the one based on the EfI value picked the field points in a somewhat balanced way. Using these hologram surfaces, source velocity distributions were recalculated adopting the same regularization method, i.e., the Tikhonov regularization technique and the GCV method. The reconstruction results recovered from the 9°-tilted hologram plane are compared in Fig. 10. Because the removal of 14 field points was made from the initial 49 field points, which are identical to the number of source points, a drastic improvement of the restored source image as illustrated in Fig. 6 was not expected; however, at least a small enhancement of the source image was expected in comparison with the case in Fig. 8(c).

In Fig. 10(a), the restored result after simply removing 14 field points located at the farthest distances is shown, which is far better than the result in Fig. 8(c). However, there still remains a question about whether the distance from the source is the best criterion in determining the meaningful position in collecting the effective field data for the reconstruction. Although the source-to-sensor distance is one important factor, but, due to the irregularity of source shape, the sound field can be very complex so that the wave front does not always follow the source shape in a conformal way. This means that the field points selection based on the distance criterion cannot assure the successful reconstruction for all cases. In this regard, the field point selection criteria based on the condition number or the EfI value can offer a reliable way in choosing the most meaningful field points for a given number of points. Fig. 10(b) and (c) show the reconstructed source velocity from the underdetermined 9°-tilted hologram plane, in which sensor positions were selected from the aforementioned reduction criteria.

The foregoing facts were studied further in depth by using the generated field pressure data. After predicting the sound field from the measured source distribution, the white noise with a SNR of 20 dB was added to the field data. In total, there were 100 sets of field pressure data. Then, from this data, source velocities at 49 surface points were reconstructed without regularization. The result is presented in Fig. 11, in which the black and grey points represent the measured and the reconstructed source velocity in complex domain, respectively. From the data scatter area, indicated in a grey zone, which is composed of 49 by 100 points, one finds that the area given by the modified hologram surfaces are far smaller than that by the original tilted hologram plane. The ratio of the data scatter areas in Fig. 11(b)–(d) to that in Fig. 11(a) are 17%, 21%, and 28%, respectively. This means that the reconstruction from the non-conformally measured data can be improved by

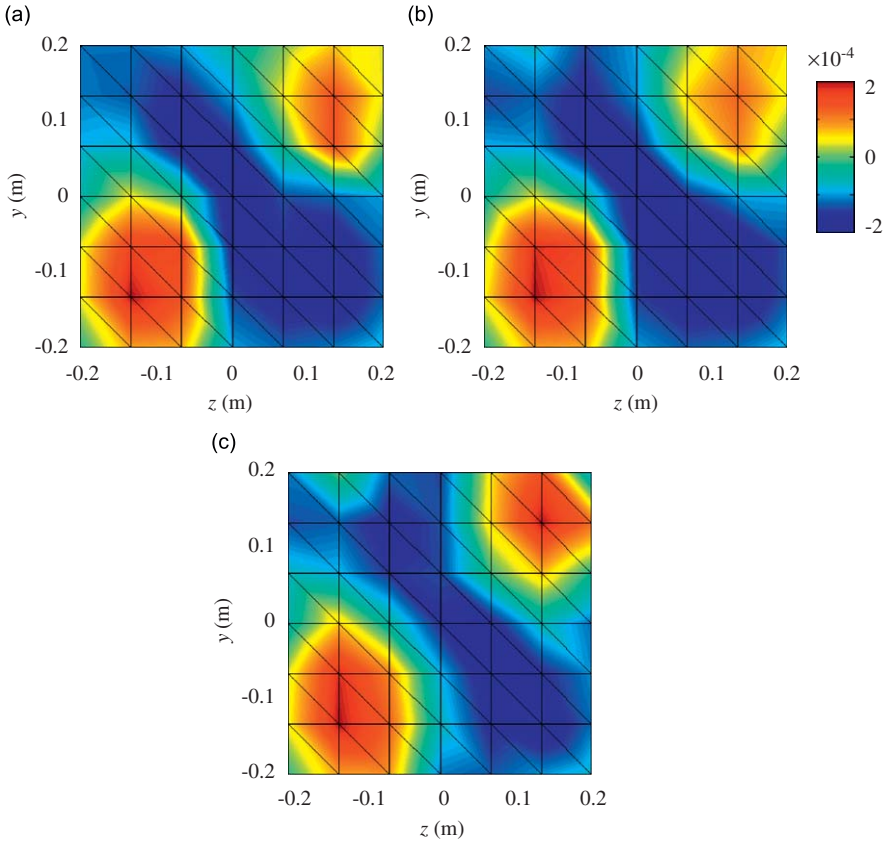

Fig. 10. The reconstructed source velocity from the underdetermined 35 field points over a hologram surface tilted by 9°, which were selected by using the three data reduction criteria from initial 49 field points. Field points were successively discarded if a field point is characterized by: (a) the farthest distance from the source (e=27%, MAC=0.86), (b) the largest condition number (e=27%, MAC=0.84), and (c) the smallest EfI value (e=28%, MAC=0.80).

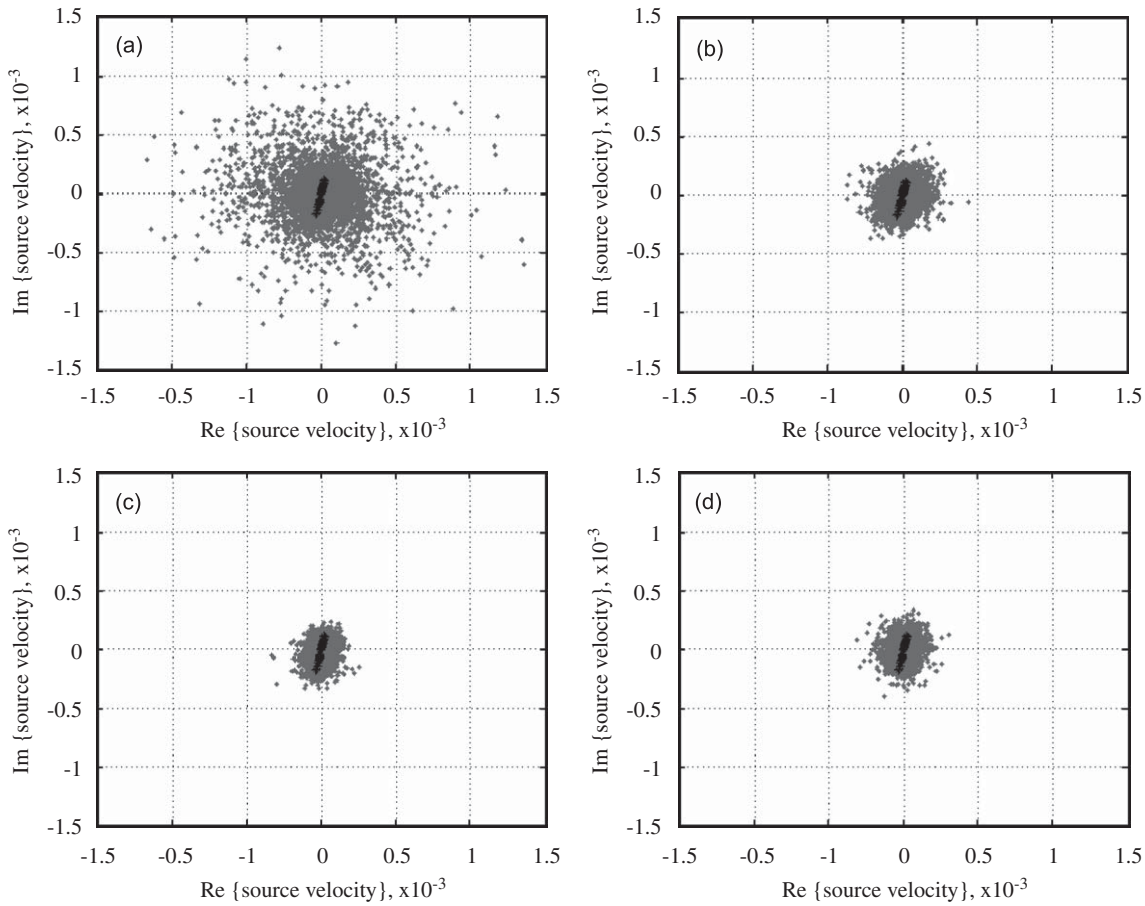

Fig. 11. A comparison of measured (✳) and reconstructed (✦) source velocity. The reconstruction was made without regularization at 49 nodes on the vibrating plates in complex coordinate using 100 field data sets given by (a) the 9°-tilted hologram surface of 49 field points. The modified hologram surfaces having 35 field points were selected by using: (b) farthest distance, (c) largest condition number, and (d) smallest EfI value.

a proper selection of field points. In this simulation, the field-point selection based on the condition number yields the best result, but the result based on the EfI value is not very much different from it. However, to remove M field points from a mother population of m field points ($M < m$), the method based on the condition number calls for $m!/M!$ calculation cycles to cover all the possible transfer functions, whereas the EfI method requires only M cycles if the points are removed one by one. If a small group of points are removed at a time using the EfI method, the amount of calculations would be some more small.

Further improvement could be achieved by applying the Tikhonov regularization technique as demonstrated in Fig. 12. The grey area becomes narrow and converges to the 49 points clustered within a compact zone. The ratio of the scatter areas associated with the modified tilted hologram planes to the original one are 65%, 61%, and 86%, respectively. This reveals that the reconstruction using the EfI-selected field points comes up with the smallest scatter area. The optimal regularization parameters, λ, for the initial tilted hologram plane and the three modified ones were calculated as 1.31, 1.01, 1.03, and 1.10, respectively. Again, these values were obtained using the GCV technique for optimal regularization parameters. It should be reminded that large regularization parameter indicates that lots of information is removed from the measured field data by the regularization. Referring to this fact, it can be said that the prejudicial selection of field points yields actually a similar effect as the regularization by truncating the redundant field points. In comparison with the initial reconstruction result as shown in Fig. 11(a), the reduction of the scatter area resulted from the combined use of field point selection and regularization technique are 45%, 62%, 67%, and 53%, corresponding to Fig. 12(a)–(d), respectively. Consequently, one can conclude that the field point selection, or screening, in other words, method based on EfI value yields the best result in terms of computation time and reconstruction error.

Table 1 summarized the reconstruction errors for the situations as described in Figs. 8 and 10 at two frequencies of 86 and 128 Hz. Two tilted hologram planes with tilting angles of 9° and 18°, as discussed in Fig. 8, were compared with the flat hologram surface cases and the number of field data was also varied. The tilted hologram plane with a tilting angle of 18° is unrealistic, but it was included to show the worst case. If the MAC score is concerned, one can find that relative strength

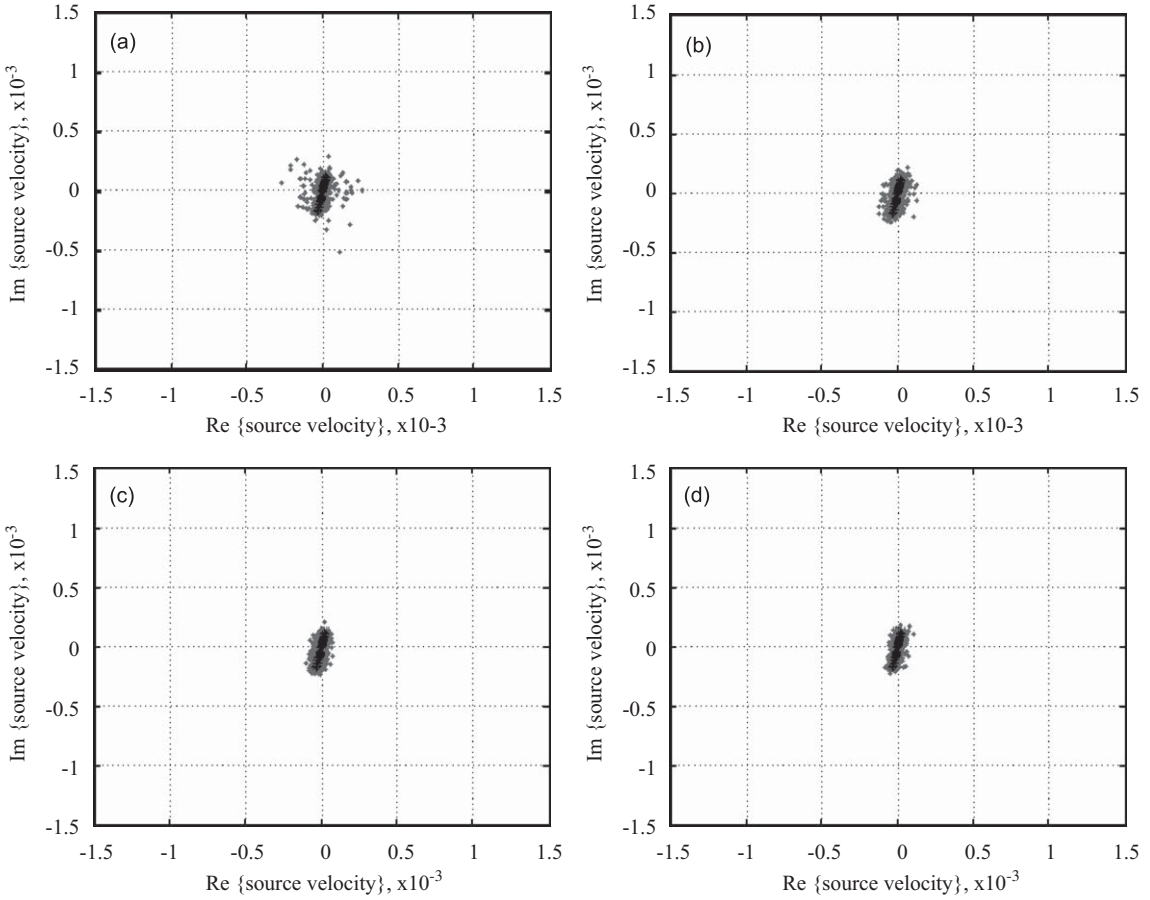

Fig. 12. A comparison of measured (✱) and reconstructed (✦) source velocity. The reconstruction was made without regularization at 49 nodes on the vibrating plates in complex coordinate using 100 field data sets given by (a) the 9°-tilted hologram surface of 49 field points (λ=1.31). The modified hologram surfaces having 35 field points were selected by using: (b) farthest distance (λ=1.01), (c) largest condition number (λ=1.03), and (d) smallest Efl value (λ=1.10).

Table 1
Reconstruction error in terms of error norm (percent) and MAC score given by the flat and the tilted hologram planes. In the tilted hologram planes, 35 field points were reduced from the initial 49 field points by removing 14 hologram data based on the three criteria: distance (Dist.), condition number (CN), and effective independence value (Efl).

Freq. (Hz)	Reconstruction error (%)						MAC score					
	49 points			35 points, tilted			49 points			35 points, tilted		
	Flat	Tilted		Dist.	CN	Efl	Flat	Tilted		Dist.	CN	Efl
86	26	9°	32	27	27	28	0.97	9°	0.63	0.86	0.84	0.80
	26	18°	2200	91	76	76	0.97	18°	0.00	0.08	0.11	0.12
128	29	9°	47	31	31	32	0.84	9°	0.36	0.73	0.76	0.76
	29	18°	1200	115	39	83	0.84	18°	0.00	0.05	0.54	0.08

and phase distribution of the source activity cannot be recovered well from the hologram surface tilted by 18°, regardless of the data selection methods. This contrasts with the result for 9°-tilted plane case. In the latter hologram surface case, both error norm and MAC value were nearly comparable to the recovered source image from the flat hologram surface, although its mean distance is longer than the flat hologram surface. Compared with restored source data from the same tilted hologram plane, but using 49 field points as shown in Fig. 8(c), error norm was changed by about 15% and MAC value by about 0.37 or two folds at 128 Hz. In this table, it seems that the data reduction method discarding the field points causing a high value of system condition number is optimal, but the difference is not big compared with the other methods. It is thought that searching for the best data reduction method should be continued. Also, the investigation on

the maximum allowable tilting angle of the hologram surface in the view point of the MAC score would give an insight about the proper measurement setup in practical measurement situations.

5. Conclusions

Effect of sensor proximity and non-conformal hologram surface to the reconstruction accuracy has been studied. As the source-to-sensor distance increases, the information containing the detailed source activity is transmitted to the sensors on the hologram surface in a diminished way. Therefore, the best way to implement the acoustical holography is to employ a conformal hologram surface. However, in practice, most sound sources are irregularly shaped source, so the hologram surface cannot be conformal to the source surface. Because the distances between source surface and nearest measuring point are various in the measurement of an irregular shaped source, the reconstruction error associated with such spatial variation of measuring distances should be investigated for the practical applications. To investigate the effect of non-conformal hologram data, simulation and measurement were conducted for an interior problem comprised of a parallelepiped rigid box except a vibrating end plate. Flat, tilted, and randomized hologram surfaces were adopted in the test.

It was shown that the reconstruction error is mostly affected by the measured field pressure at the positions located far from the source surface and the quality of reconstructed source image is affected largely from the nearest field data. To improve the reconstruction accuracy, an investigation was conducted to find proper field points among a number of overdetermined field points which were initially considered as possible candidate positions for the measuring sensors. The number of field data was reduced gradually under several reduction schemes: discarding the data point if the condition number is largest of all or the EfI value is smallest of all or the distance from the source surface is the longest of all. We could not find any dramatic improvement of the reconstruction accuracy by reducing a number of field points from the mother population of field points in the overdetermined situation. However, by continuing the reduction process to construct an underdetermined situation, a drastic improvement of the reconstruction accuracy could be observed for the test frequency and model that were used in this paper. For a tilted hologram plane by 9°, error norm was changed by about 15% and MAC value by about 0.37 or two folds at a frequency. However, this does not suggest that the underdetermined measurement condition will always improve the reconstruction accuracy. One should remind that the data reduction was started from a very large candidate field points initially, so the underdetermined condition producing a significant enhancement of the reconstruction was very selectively chosen from this large overdetermined population. Consequently, the arrangement of hologram data by a proper selection of field points to remove non-unique measurements can be considered as one of regularization approaches that improves the solution.

Acknowledgments

This work was partially supported by the Korea Research Fund (KRF) and BK21 Project.

Appendix A. Additional explanation on Fig. 6

In Fig. 6, the initial hologram data comprised of 94 field points contains a lot of measurement points having redundant information. By gradually eliminating field points from a large initial population of field data, the condition number has a firstly decreasing trend before reaching the demarcation between overdetermined and underdetermined condition. Because the redundant information is removed from the matrix by a proper selection of eliminating points, the condition number naturally decreases by the reduction of matrix size. Another decreasing trend can be observed in the underdetermined situation due to the fact that the problem has a fewer number of constraints than the overdetermined situation reducing the difference between maximum and minimum singular values. Note that the measured field data is a kind of constraints in solving the inverse problem at hand.

Actually, we started from a highly overdetermined situation with many candidate field points, and then, by the geometric relationship between source and field points, the field points that offer the most independent information were selected for a given number of field points during the elimination procedure. Therefore, the choice of field points from an underdetermined situation is actually based on the initial full population of field points; that means the method is still based on the overdetermined problem.

The sudden increase of CN at around 50 field points is not thought to be related to either BEM calculation or field point selection techniques. To find the reason why does the singularity of the system increase sharply when the number of field points approaches the number of source points, a simple numerical test was conducted. Initially, 50 rectangular $m \times n$ matrices are generated in a random manner. Now, define the size of initial matrices as $m=50$ and $n=75$. Starting with these 50 random, 50×75 matrices, the size of matrix is reduced one by one until it reaches 50×25. The maximum singular value as displayed in Fig. A1(a) shows a monotonic decrease with a gradual elimination of matrix column n. On the other hand, the minimum singular value as shown in Fig. A1(b) has a slight decreasing and then increasing trend that has a trough when the matrix size is 50×50. The singular values of 50 random 50×50 matrices are ranged from 0.0013 to 0.0753.

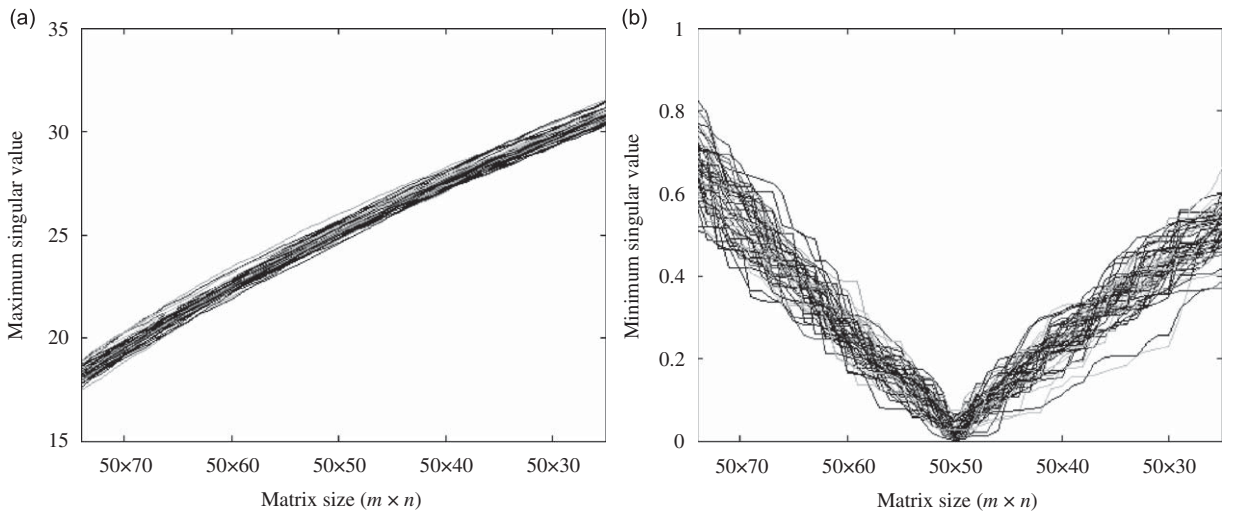

Fig. A1. Singular values from 50 random matrices by reducing the matrix column one by one: (a) maximum singular value and (b) minimum singular value. At the matrix size of 50×50, the minimum singular values are ranged from 0.0013 to 0.0753.

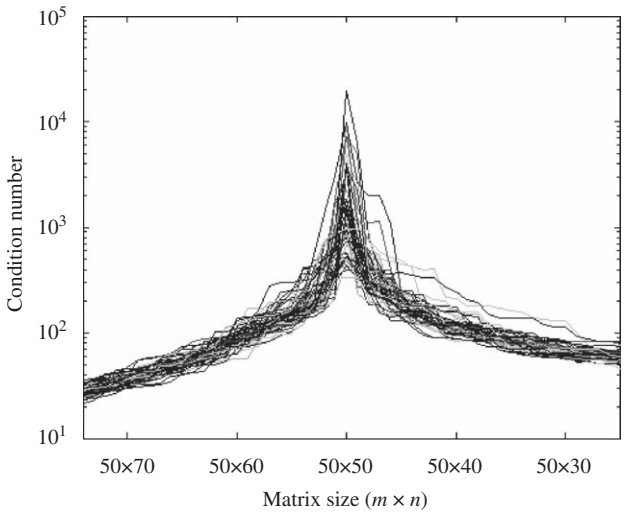

Fig. A2. Condition number calculated by SVD from 50 random matrices. Peak values exist at the matrix size of 50×50.

Fig. A2 shows the condition number, by taking the ratio of the maximum to the minimum singular values, which exhibits a peak at 50×50 in matrix size.

The procedure in finding an inverse solution for a system of $\mathbf{p}_{(m\times 1)}=\mathbf{G}_{(m\times n)}\mathbf{v}_{(n\times 1)}$ involves a pseudo-inverse calculation of $\mathbf{G}(\mathbf{G}^{\mathrm{T}}\mathbf{G})^{-1}\mathbf{G}^{\mathrm{T}}$. Here, $\mathbf{G}$ and $\mathbf{G}(\mathbf{G}^{\mathrm{T}}\mathbf{G})^{-1}\mathbf{G}^{\mathrm{T}}$ share the same null space. Then, the singular values of $\mathbf{G}$ are provided by SVD by taking the square root of the eigenvalues of $\mathbf{G}^{\mathrm{T}}\mathbf{G}$. The null-space is determined by choosing a zero bound of the singular values. This means that when $m > n$, the SVD has a wider option to choose which element can be treated as zero in such a way to minimize $\|\mathbf{p}-\mathbf{G}\mathbf{v}\|^2$. Therefore, when the matrix size is changed from 50×50 to 50×51, SVD can choose a higher zero bound that result a larger minimum singular value. Actually, the maximum singular value also increases with the matrix size, but, because the change of minimum singular value is more drastic than the maximum singular value, the condition number decreases. This situation is also true for the other cases of increasing matrix size, e.g. 50×51, 50×52, etc. Thus, the trend of condition number is decreasing in this overdetermined case. It should be noted that the matrices used in the simulation are different in character compared to the actual measured data; 50 matrices are randomly built, so they do not have coherency at all. The simulation is thus characterizing the general attribute of the ill-conditioned matrix only.

Summarizing the foregoing two mechanisms, the condition number decreases first with the reduction of the transfer matrix size by using a proper elimination of field points, because a large overdetermined data points measured over the hologram contain lots of redundant information. After most of the redundant information is removed by eliminating many

properly chosen field points, the condition number starts to increase because the zero bound increases due to the inherent character of the matrix system as discussed above. Then, shortly after passing the point where the number of field points is equal to the number of source points, the condition number decreases again because the problem has a fewer number of constraints than the overdetermined situation reducing the difference between maximum and minimum singular values.

References

[1] W. Dijkstra, R.M.M. Mattheij, The condition number of the BEM matrix arising from Laplace's equation, *Electronic Journal of Boundary Elements* 4 (2006) 67–81.
[2] H.L. Kuntz, Radiated sound and the geometric nearfield size, *Noise Control Engineering Journal* 56 (2008) 269–281.
[3] E.G. Williams, J.D. Maynard, Holographic imaging without the wavelength resolution limit, *Physical Review Letters* 45 (1980) 554–557.
[4] B.-U. Koo, B.-C. Lee, J.-G. Ih, A non-singular boundary integral equation for acoustic problems, *Journal of Sound and Vibration* 192 (1996) 263–279.
[5] S.-C. Kang, J.-G. Ih, Use of non-singular boundary integral formulation for reducing errors due to near-field measurements in the boundary element method based near-field acoustic holography, *Journal of Acoustical Society of America* 109 (2001) 1320–1328.
[6] K.-U. Nam, Y.-H. Kim, Errors due to sensor and position mismatch in planar acoustic holography, *Journal of Acoustical Society of America* 106 (1999) 1655–1665.
[7] B.-K. Kim, J.-G. Ih, On the reconstruction of the vibro-acoustic field over the surface enclosing an interior space using the boundary element method, *Journal of Acoustical Society of America* 100 (1996) 3003–3016.
[8] F. Seybert, B. Soenarko, F.J. Rizzo, D.J. Shippy, An advanced computational method for radiation and scattering of acoustic waves in three dimensions, *Journal of Acoustical Society of America* 77 (1985) 362–368.
[9] B.-K. Kim, J.-G. Ih, Design of an optimal wave-vector filter for enhancing the resolution of reconstructed source field by near-field acoustical holography (NAH), *Journal of Acoustical Society of America* 107 (2000) 3289–3297.
[10] E.G. Williams, Regularization methods for near-field acoustical holography, *Journal of Acoustical Society of America* 110 (2001) 1976–1988.
[11] Y. Kim, P.A. Nelson, Optimal regularization for acoustic source reconstruction by inverse methods, *Journal of Sound and Vibration* 275 (2004) 463–487.
[12] R. Upton, K. Haddad, J. Sorensen, Conformal mapping techniques for consumer products, Sound and Vibration, July 2008.
[13] S. Marburg, Six boundary elements per wavelength: is that enough?, *Journal of Computational Acoustics* 10 (2002) 25–52.
[14] P.A. Nelson, S.H. Yoon, Estimation of acoustic source strength by inverse methods: Part I, conditioning of the inverse problem, *Journal of Sound and Vibration* 233 (2000) 643–668.
[15] A. Schuhmacher, J. Hald, K.B. Rasmussen, P.C. Hansen, Sound source reconstruction using inverse boundary element calculation, *Journal of Acoustical Society of America* 113 (2003) 114–127.
[16] R.J. Allemang, D.L. Brown, A correlation coefficient for modal vector analysis, In *Proceedings of the 1st International Modal Analysis Conference*, 1982, pp. 110–116.
[17] F. Martinus, D.W. Herrin, A.F. Seybert, Selecting measurement locations to minimize reconstruction error using the inverse boundary element method, *Journal of Computational Acoustics* 15 (2007) 531–555.
[18] N. Thite, D.J. Thompson, Selection of response measurement locations to improve inverse force determination, *Applied Acoustics* 67 (2006) 797–818.
[19] Z. Zhang, N. Vlahopoulos, S.T. Raveendra, T. Allen, K.Y. Zhang, A computational acoustic field reconstruction process based on an indirect boundary element formulation, *Journal of Acoustical Society of America* 108 (2000) 2167–2176.
[20] D.C. Kammer, Sensor placement for on-orbit modal identification and correlation of large space structures, *Journal of Guidance, Control, and Dynamics* 14 (1991) 251–259.
[21] J.-G. Ih, Inverse boundary element techniques for the holographic identification of vibro-acoustic source parameters, in: S. Marburg, B. Nolte (Eds.), *Computational Acoustics of Noise Propagation in Fluids*, Springer, Berlin, 2008 (Chapter 20).